VRIJE
UNIVERSITEIT
BRUSSEL

Determination of the radial profile of the photoelastic coefficient of polymer optical fibers

Acheroy, S.; Merken, P.; Geernaert, Thomas; Ottevaere, Heidi; Thienpont, Hugo; Berghmans, Francis

Document Version:
Final published version

Link to publication

Determination of the radial profile of the photoelastic coefficient of polymer optical fibers

Sophie Acheroy*[a], Patrick Merken[a], Thomas Geernaert[b], Heidi Ottevaere[b], Hugo Thienpont[b], Francis Berghmans[b]

[a]Royal Military Academy, Dept of Communication, Information, Systems and Sensors (CISS), Ave Renaissance 30, 1000 Brussels, Belgium; [b]Vrije Universiteit Brussel, Dept. of Applied Physics and Photonics, Brussels Photonics Team (B-PHOT), Pleinlaan 2, B-1050 Brussels, Belgium

ABSTRACT

We determine the radial profile of the photoelastic constant C(r) in two single mode and one multimode polymer optical fibers (POFs), all fabricated from polymethylmethacrylate (PMMA). To determine C(r) we first determine the retardance of the laterally illuminated fiber submitted to a known tensile stress uniformly distributed over the fiber cross-section. Then we determine the inverse Abel transform of the measured retardance to finally obtain C(r). We compare two algorithms based on the Fourier theory to perform the inverse transform. We obtain disparate distributions of C(r) in the three fibers. The mean value of C(r) varies from -7.6×10^{-14} to 5.4×10^{-12} Pa^{-1}. This indicates that, in contrast to glass fibers, the radial profile of the photoelastic constant can considerable vary depending on the type and treatment of POFs, even when made from similar materials, and hence the photoelastic constant should be measured for each type of POF.

Keywords: Polymer optical fiber, inverse Abel transform, photoelastic constant, fiber characterization

1. INTRODUCTION

Polymer optical fibers (POFs) are gaining interest in the field of optical fiber sensors. Compared to regular silica optical fiber based sensors, POFs can provide high elastic strain limits and can be biocompatible [1–3]. Fiber optic sensors used for measuring mechanical quantities such as strain and pressure often exploit the photoelastic effect. Photoelasticity is the basis for the stress-optic law that establishes the link between applied stress and induced birefringence. It uses the photoelastic constant C as material dependent coefficient [4]. The material we focus on in this article is polymethylmethacrylate (PMMA), as PMMA is actually the most commonly used polymer for fabricating POFs. For PMMA, the value of C reported in the literature varies significantly, from -1.08×10^{-10} Pa^{-1} to 5.3×10^{-12} Pa^{-1} [5–10]. Moreover the photoelastic constant in PMMA also depends on the presence and concentration of dopants in the polymer and on the drawing conditions of the polymer fiber. This may point at the necessity to measure C for every different type of POF. In addition, all the methods that have been proposed so far to determine C in glass and polymer fibers rely on the hypothesis that C is constant over the core cross-section of the fiber [11,12]. Considering the fabrication method of optical fibers, making that assumption is not necessarily straightforward. We therefore also discuss the radial profile of the photoelastic coefficient C(r) in PMMA based POF. In section 2 we describe the measurement method and two algorithms that we have implemented to determine C(r) in optical fibers. The actual measurement results on the POFs are presented and discussed in the third section. We compare the convergence and robustness of the radial distribution profiles of the photoelastic constant obtained with both algorithms. Section 4 closes our article with a summary of our findings.

2. DESCRIPTION OF THE MEASUREMENT METHOD

2.1 Retardance measurement

The determination of C(r) requires the measurement of the retardance profile of a transversally illuminated fiber as a function of the tensile load applied to the fiber. The inverse Abel transform of the retardance allows obtaining C(r). In previous publications we have detailed a measurement method to obtain the retardance profile of the fiber [13,14]. We recall the main steps below for the sake of completeness.

We subject the fiber to a known axial load σ_z. We assume the load is constant over the fiber section. The fiber is illuminated with monochromatic light at 633 nm, linearly polarized light at 45°C with respect to the fiber axis. As illustrated in Figure 1 the wave vector of the light is perpendicular to the fiber axis and parallel with the x-axis. The fiber is immersed in index matching liquid to avoid refraction at the boundaries of the optical fiber.
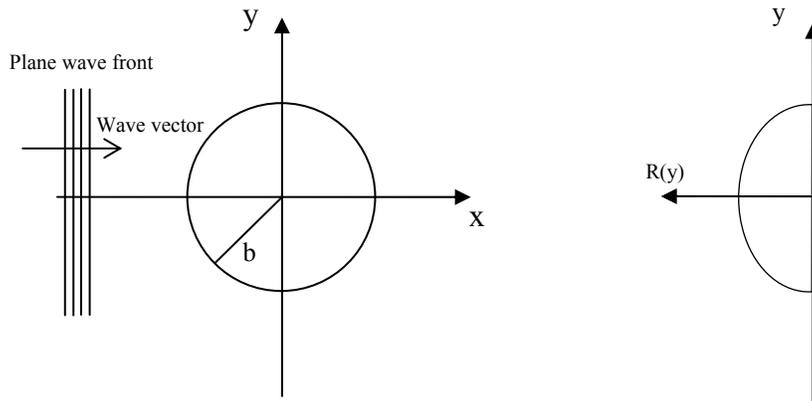

Figure 1: Illustration of an optical fiber transversely illuminated with a plane wave (left) and resulting retardance profile R(y) (right). b is the radius of the fiber. The z-axis is taken along the fiber length with a direction exiting the page.

The axial load applied to the fiber induces birefringence in the fiber material. The two linearly polarized components along the y and z directions will experience a different phase shift that can be observed as the projected retardance R(y) between these two orthogonal components. The projected retardance R(y) is related to the axial stress by an inverse Abel transform [15–17], as given by equation (1):

$$\sigma_z \times C(r) = -\frac{1}{\pi} \int_r^b \frac{dR(y)/dy}{\sqrt{y^2 - r^2}} \, dy \tag{1}$$

The photo-elastic constant C(r) is the regression coefficient linking the inverse Abel transform of the projected retardance R(y) and the applied known axial stress σ_z. r is the radial distance taken from the fiber's center and b is the radius of the fiber. To obtain the radial profile of the photoelastic constant C(r), we use a polarizing microscope and apply the Sénarmont compensation method to measure the full-field view of R(y). The set-up is illustrated in Figure 2.

The optical fiber is placed between a polarizer and quarter wave plate aligned at 45° with respect to the fiber's axis. The birefringence of the fiber causes the orientation of the linearly polarized light to change at the output of the quarter wave plate. The analyzer is oriented perpendicularly to that direction, which results in extinction of the light exiting the analyzer. The angular range of rotation of the analyzer θ_{Atot} is chosen to achieve extinction for every pixel in the field of view of the microscope.
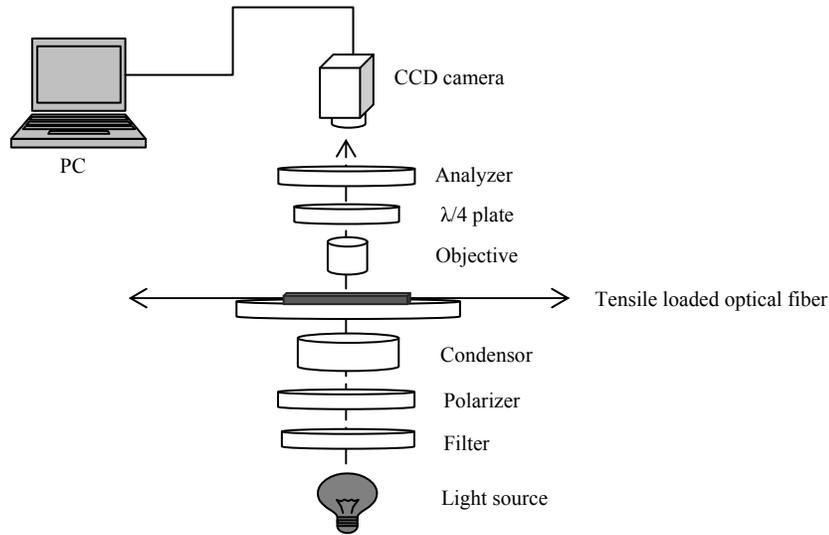
Figure 2: Polarization microscope set-up to measure the full-field retardance profile using the Sénarmont compensation method. To obtain a controlled tensile stress, a predefined axial load is applied to the fiber using an external loading system.

A CCD camera records an image for each position of the analyzer θ_A in that range. For each pixel the recorded intensity is plotted as a function of θ_A. A polynomial fit is performed on the intensity profile to determine the minimal intensity and the corresponding analyzer angle $\theta_{A\min}$. The retardance in the pixel under consideration is determined with

$R(y) = \dfrac{\theta_{A\min}}{180} \lambda$ with $\theta_{A\min}$ in degrees. We used objective lenses with 20x magnification and numerical apertures of 0.50, resulting in spatial resolutions of 0.77 µm. This is sufficient to obtain radial profiles taking into account the typical dimensions of the optical fibers.

2.2 Inverse Abel transform

In our previous publication [18] we introduced two algorithms to compute the inverse Abel transform. Both algorithms are based on Fourier theory but the approach is different. With the first algorithm we expand the measured retardance R(y), corresponding to a specific value of the axial load, in Fourier series. We compute the inverse Abel transform of the expansion of R(y) and we obtain equation (2).

$$\sigma_z \times C(r) = -\frac{\pi}{2b} \sum_{k=1}^{k\max} a_k k \frac{2}{\pi} \int_0^{\sqrt{1-\rho^2}} (t^2 + \rho^2)^{-1/2} \times \sin(k\pi\sqrt{t^2 + \rho^2})dt \qquad (2)$$

where $\rho = r/b$ is the normalized radius, $t = \sqrt{1-\rho^2}$ and a_k is the kth Fourier coefficient of the Fourier series of the retardance.

With the second algorithm we expand the result $C(r).\sigma_z$ of the inverse Abel transform in Fourier series. The expression of the expansion is given in equation (3).

$$\left[\sigma_z \times C(r)\right]_F = a_0 + \sum_{k=1}^{\infty} a_k \cos(k\pi\frac{r}{b}) \qquad (3)$$

The forward Abel transform of the expansion allows obtaining the measured retardance. The expression of the retardance becomes (4).

$$R_F(y) = b.a_0 \int_0^{\sqrt{1-\rho^2}} dt + b\sum_{k=1}^{\infty} a_k \int_0^{\sqrt{1-\rho^2}} \cos(k\pi\sqrt{t^2 + \rho^2})dt \tag{4}$$

where $\rho = x/b$ is the normalized radius and $t = \dfrac{\sqrt{r^2 - y^2}}{b}$. To determine the amplitude of the Fourier coefficients a_k in

equation (4), $R_F(y)$ is compared to the measured retardance by applying the least square criterion.

The main difference between the two algorithms is the presence of a constant term in the expansion of $\sigma_z \times C(r)$ in the second algorithm. It allows the algorithm to converge with a lower amount of Fourier coefficients. Moreover, the first algorithm requires the integration of a derivative, which is very sensitive to measurement noise. To establish the radial distribution of the photoelastic constant, we have demonstrated in [18] that both algorithms are fully equivalent, but that the first algorithm requires a larger amount of Fourier coefficients. If we consider increased measurement noise, the influence of the noise on the inverse Abel transform becomes predominant and a large number of Fourier coefficients leads to very noisy shapes. In that case the amount of considered coefficients has to be reduced and C(r) should then be calculated with the second algorithm.

3. MEASUREMENT RESULTS AND DISCUSSION

We measure C(r) of two singlemode and one multimode polymer fibers. The main characteristics of the fibers are summarized in Table 1. We measure the retardance for tensile stress values varying from 10 MPa to 50 MPa.

Table 1: Main characteristics of the polymer optical fibers used to measure the retardance and determine the radial profile of the photoelastic coefficient [19–21].

Fiber	Type	Mode	d_{core}	$d_{cladding}$	n_{core}	$n_{cladding}$
1	PMMA	Singlemode	5,94 μm	110 μm	1,4919	1,4905
2	PMMA	Singlemode	12 μm	260 μm	1,4919	1,4905
3	PMMA	Multimode	240 μm	245 μm	1,49	1,402

We use two approaches to determine the photoelastic constant. First we substitute the measured retardance with a half ellipse. If we consider a tensile stress σ_z uniformly distributed over the fiber cross-section and assume C to be constant over that section, the retardance has indeed an elliptical shape. The analytical expression of the inverse Abel transform of the semi-ellipse is solely function of the semi-long axis and the semi-short axis of the semi-ellipse, i.e. respectively the radius of the fiber b and the maximum absolute value of R(y). The relation between the applied tensile stress and the measured retardance becomes (equation (5)) [14]:

$$\sigma_z \times C = -\frac{1}{2}\frac{\max(abs(R(y)))}{b} \tag{5}$$

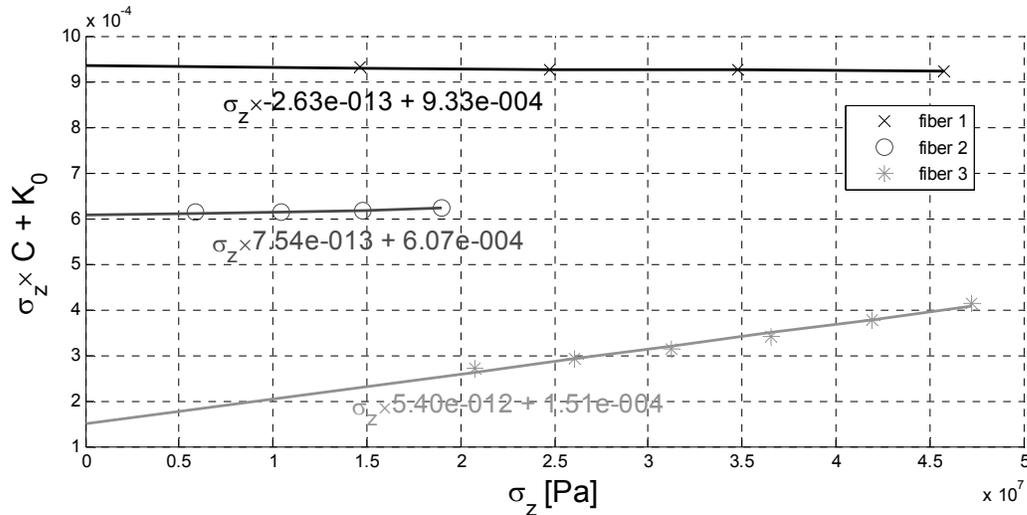C is the regression coefficient we have to determine. The results we obtain with this method are shown inFigure 3.

Figure 3: C .σ_z as a function of the axial stress. The regression coefficient is the photoelastic constant C. Its values are indicated in the graph along the respective linear fits.

The elliptical approximation allows determining the mean value of the photoelastic constant. We obtain values for C of -2.62×10^{-13} Pa^{-1} for fiber 1, 7.54×10^{-13} Pa^{-1} for fiber 2 and 5.40×10^{-12} Pa^{-1} for fiber 3.

The second approach consists in determining the radial distribution of the photoelastic constant without any approximation. We compute the inverse Abel transform of the measured retardance corresponding to a specific tensile stress using both algorithms described in section 2.2.

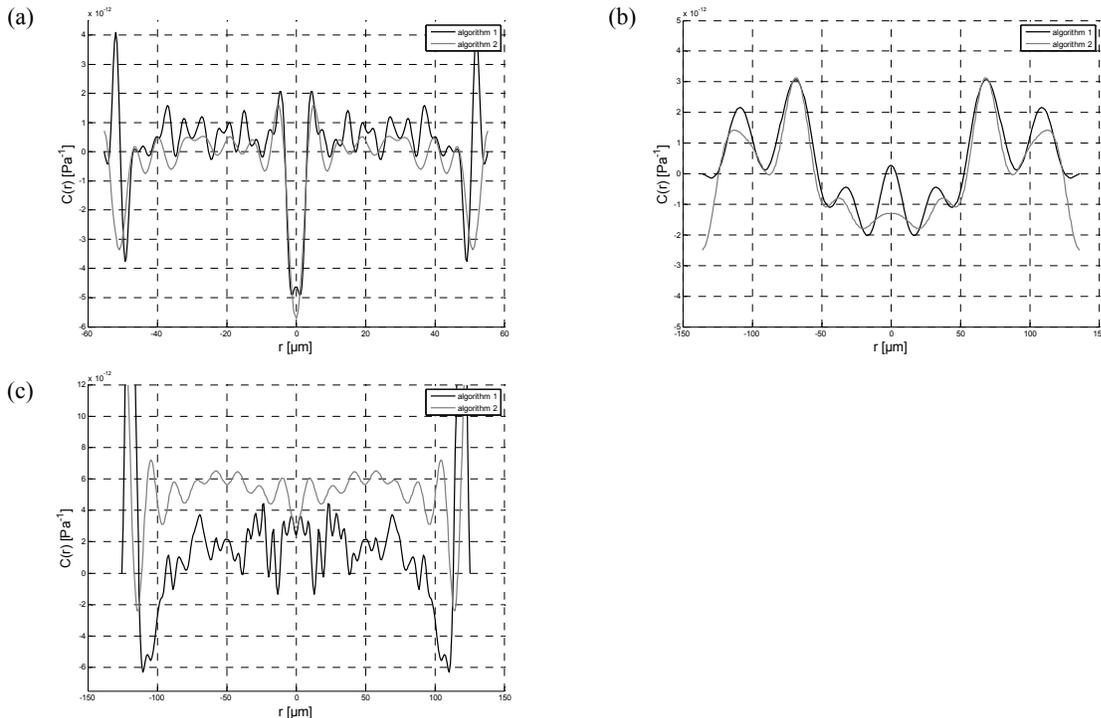Figure 4: Radial distribution of the photoelastic constant C(r) in one fiber section. The profiles are respectively computed with the first and the second algorithm. (a) C(r) in fiber 1 with the amount of Fourier coefficients $k_{algorithm\ 1} = 31$ and $k_{algorithm2} = 15$, (b) C(r) in fiber 2 with $k_{algorithm\ 1} = k_{algorithm2} = 10$ and (c) C(r) in fiber 3 with $k_{algorithm\ 1} = 49$ and $k_{algorithm2} = 15$.

This allows obtaining the relationship $f(r) = \sigma_z \times C(r)$. Finally the linear regression of $f(r)$ is computed for every radial point to obtain the radial distribution of the photoelastic constant C(r). Figure 4 shows the radial profile of the photoelastic constant for the three polymer fibers. The radial profile of C(r) in fiber 1 is stable, except in the center and at the edges of the fiber. The overshoots are due to mathematical artefacts of the inverse Abel transform. For fiber 2 the profile is very oscillatory and the value of C(r) is very small. This might indicate that the overall value of C(r) is lost in the measurement noise and variance of the inverse Abel algorithm. The results with both algorithms are comparable. The measurement noise on fiber 3 is quite high. As a consequence the profile of C(r) determined with the first algorithm is very noisy and it does not converge towards the shape of the radial distribution of C(r) obtained using the second algorithm. The results for fiber 3 tend to prove that the second algorithm is very robust when one has to cope with the inverse Abel transform of a noisy profile. The mean values of C taken in the stable portions of C(r) are respectively -7.6×10^{-14} Pa^{-1} for fiber 1, 6.0×10^{-13} Pa^{-1} for fiber 2 and 5.4×10^{-12} Pa^{-1} for fiber 3, i.e. close to the values found with the elliptical method. These values differ significantly and the overall shape of the profiles are not identical. Moreover, the values measured in the two singlemode fibers are clearly much smaller than in the multimode fiber. This finding can be explained by the strong dependence of the photoelastic constant of a polymer fiber on the fabrication and production process [22]. Note that we obtain identical results for different lengths of fiber taken from the same fabrication batch. C(r) should therefore be measured for each type of fiber, but measuring one fiber sample from a single fabrication seems sufficient to determine the photoelastic coefficient of that specific POF.

4. CONCLUSIONS

We measured the radial distribution of the photoelastic constant in three types of PMMA optical fibers. We first have to determine the retardance of the laterally illuminated fiber. We use a polarizing microscope to obtain a full field of view of the retardance. We apply two algorithms based on the Fourier theory to perform the inverse Abel transform of the measured retardance. The first algorithm decomposes the measured retardance in Fourier series before to performing the inverse Abel transform, whilst the second algorithm expands the desired radial profile and then computes the forward Abel transform. The result of that operation is then compared to the measured retardance profile. The main conclusion is that the second algorithm is more robust when one has to deal with noisy data.

We measure a mean value of C that equals -7.6×10^{-14} Pa^{-1} and 6.0×10^{-13} Pa^{-1} in the singlemode fibers 1 and 2, and 5.4×10^{-12} Pa^{-1} in the multimode fiber 3. The photoelastic coefficients of the PMMA fibers under test are therefore very different, which indicates that C cannot be approximated by any 'standard' value, but that it should be measured for every single type of POF.

REFERENCES

[1]   N. G. Harbach, "Fiber bragg gratings in Polymer Optical Fibers," 118 (2008).
[2]   K. Peeters, "Polymer optical fibre sensors - A review," *Smart Mater. Struct.* **20**(013002), IOP Publishing (2011) [doi:10.1088/0964-1726/20/1/013002].
[3]   F. Berghmans and H. Thienpont, "Plastic Optical Fibers for Sensing Applications," 3–5 (2014).
[4]   K. J. Gadvik, *Optical metrology*, Third Edit, Wiley & Sons, LTD (2002).
[5]   A. Tagaya, L. Lou, Y. Ide, Y. Koike, and Y. Okamoto, "Improvement of the physical properties of poly(methyl methacrylate) by copolymerization with N-pentafluorophenyl maleimide; zero-orientational and photoelastic birefringence polymers with high glass transition temperatures," *Sci. China Chem.* **55**(5), 850–853 (2012) [doi:10.1007/s11426-012-4498-9].
[6]   A. Tagaya, H. Ohkita, T. Harada, K. Ishibashi, and Y. Koike, "Zero-birefringence optical polymers," *Macromolecules* **39**, 3019–3023 (2006) [doi:10.1021/ma0527000].
[7]   R. M. Waxler, D. Horowitz, and A. Feldman, "Optical and physical parameters of Plexiglas 55 and Lexan," *Appl. Opt.* **18**(1), 101–104 (1979).
[8]   W. Xu, X. F. Yao, H. Y. Yeh, and G. C. Jin, "Fracture investigation of PMMA specimen using coherent gradient sensing (CGS) technology," *Polym. Test.* **24**, 900–908 (2005).
[9]   H. Ohkita, K. Ishibashi, D. Tsurumoto, a. Tagaya, and Y. Koike, "Compensation of the photoelastic birefringence of a polymer by doping with an anisotropic molecule," *Appl. Phys. A* **81**(3), 617–620 (2005) [doi:10.1007/s00339-004-3133-9].

[10] F. Ay, A. Kocabas, C. Kocabas, A. Aydinli, and S. Agan, "Prism coupling technique investigation of elasto-optical properties of thin polymer films," *J. Appl. Phys.* **96**(12), 7147–7153 (2004).

[11] A. Bertholds and B. Dändliker, "Determination of the individual strain-optic coefficients in single-mode optical fibers," *J. Light. Technol.* **6**(n°1), 17–20 (1988).

[12] N. Lagakos and R. Mohr, "Stress optic coefficient and stress profile in optical fibers," *Appl. Opt.* **20**(13), 2309–2313 (1981).

[13] S. Acheroy, M. Patrick, G. Thomas, H. Ottevaere, H. Thienpont, and F. Berghmans, "On a possible method to measure the radial profile of the photoelastic constant in step-index optical fiber," in *Opt. Sens. Detect. III*, F. Berghmans, A. G. Mignani, and P. De Moor, Eds., Proc. of SPIE Vol. 9141, 914115 (2014) [doi:10.1117/12.2050343].

[14] S. Acheroy, P. Merken, H. Ottevaere, T. Geernaert, H. Thienpont, and F. Berghmans, "Influence of measurement noise on the determination of the radial profile of the photoelastic coefficient in step-index optical fibers.," *Appl. Opt.* **52**(35), 8451–8459 (2013).

[15] Chu and Whitbread, "Measurement of stresses in optical fiber and preform," *Appl. Opt.* **21**(23), 4241–4245 (1982).

[16] K. Tatekura, "Determination of the index profile of optical fibers from transverse interferograms using Fourier theory," *Appl. Opt.* **22**(3), 460–463 (1983).

[17] H. Poritsky, "Analysis of thermal stresses in sealed cylinders and the effect of viscous flow during anneal," *Physics (College. Park. Md).* **5**, 406–411 (1934).

[18] S. Acheroy, P. Merken, T. Geernaert, H. Ottevaere, H. Thienpont, and F. Berghmans, "Algorithms for determining the radial profile of the photoelastic coefficient in glass and polymer optical fibers," *Opt. Express* **23**(15), 18943 (2015) [doi:10.1364/OE.23.018943].

[19] "http://i-fiberoptics.com/fiber-detail.php?id=120."

[20] "http://www.paradigmoptics.com/."

[21] W. Wu, Y. Luo, X. Cheng, X. Tian, W. Qiu, B. Zhu, G. Peng, and Q. Zhang, "Design and fabrication of single mode polymer optical fiber gratings," 1652–1659 (2010).

[22] M. C. Szczurowski, T. Martynkien, G. Statkiewicz-Barabach, L. Khan, D. J. Webb, C. Ye, J. Dulieu-Barton, and W. Urbanzyck, "Measurements of stress-optic coefficient and Young's modulus in PMMA fibers drawn under different conditions," in *SPIE Photonic Cryst. Fibers IV Vol 7714*, K. Kalli and W. Urbanzyck, Eds., pp. 1–8, SPIE (2010) [doi:10.1117/12.855089].